


RESEARCH

Open Access



# A species-transport model for circulation in a leading-edge vortex

Clara Giner-Morency and Jaime G. Wong\* 

\*Correspondence:  
jgwong@ualberta.ca

Department of Mechanical  
Engineering, University  
of Alberta, Edmonton T6G 1H9,  
Canada

## Abstract

In this study, we propose a model to predict circulation growth along the span of a rotating wing, in which circulation transport is represented as species transport. Fluid particles entering the vortex shear layer at the leading edge are initialized as vorticity-containing mass and are advected by the flow along the span. A circulation budget is presented, consisting of a generation and transport term, the latter derived from the vorticity transport equation, which leaves only two unknowns for the modeller to determine: the shear-layer thickness and the spanwise flow distribution. We find that the model is insensitive to the value chosen for the shear-layer thickness, as varying the thickness by an order of magnitude only changes the output by a few percent. Meanwhile, we use Bernoulli equation in a rotating coordinates system as a basic model for spanwise flow. To verify the accuracy of the model, the predicted circulation values are compared against experimental circulation values and show good agreement to measurements close to the axis of rotation, which corresponds to the spanwise locations at which the spanwise flow model best matches experimental data. It is suggested, therefore, that this model produces accurate results subject to an appropriate spanwise flow model.

**Keywords:** Leading-edge vortices, Circulation transport, Vortex growth, Rotating wings

## 1 Introduction

Leading-edges vortices (LEVs) often present highly three-dimensional flow characteristics, which makes modeling difficult. However, understanding their dynamics is essential for understanding biological locomotion, or using such locomotion to develop engineered flyers [1–3]. The present work will provide a circulation growth model for a rotating wing that accounts for some of these three dimensional characteristics. The model will estimate the circulation distribution from the flux of circulation through the leading-edge shear layer and its transport through the spanwise flow.

### 1.1 The circulation balance of an LEV

Modelling the circulation growth of an LEV in three-dimensional flows, such as flapping or rotating wings, is challenging because the circulation at any given spanwise location and the spanwise transport of circulation at that location tend to be

coupled. For instance, many previous modelling efforts have required knowledge of the vorticity field to determine spanwise flow [4]. One possible simplification is to model circulation transport as species transport, neglecting the complex vortex tilting behaviour, when the case permits [5, 6]. In this paradigm, the circulation transport is characterized by two terms: the circulation feeding rate  $(\partial\Gamma/\partial t)_{\text{in}}$  and its spanwise transport via spanwise flow  $(\partial\Gamma/\partial t)_{\text{out}}$ . The circulation balance is thus expressed as:

$$\left(\frac{\partial\Gamma}{\partial t}\right)_{\text{total}} = \left(\frac{\partial\Gamma}{\partial t}\right)_{\text{in}} - \left(\frac{\partial\Gamma}{\partial t}\right)_{\text{out}}, \quad (1)$$

where  $\Gamma$  represents the circulation. For a stable LEV in steady state, such as that found on rotating wings, this balance must be zero. This simplification has been previously validated for a translating delta-wing, where spanwise flow is relatively constant [6].

The circulation feeding rate into the LEV is characterized by the vorticity generation within the shear-layer. As shown by Didden, a relationship can be established between the rate of circulation growth and the shear-layer velocity for a vortex generated by a piston-cylinder [7]:

$$\left(\frac{\partial\Gamma}{\partial t}\right)_{\text{in}} = \frac{1}{2}u^2, \quad (2)$$

where  $u$  is the shear-layer velocity. A numerically identical result can be obtained for an LEV formed on a wing through a distinct derivation, in which mass enters and feeds the leading edge vortex through the shear layer at the wing's leading edge, and likewise for the circulation generated in a boundary layer [6–8].

Since the circulation flux through the leading-edge shear layer depends strongly on the shear-layer velocity, the distribution of shear-layer velocity along the span must be determined. The shear-layer velocity profile has been investigated in many studies, as its evaluation is tied to the understanding of the vortex growth [6, 9, 10]. However, most of the available models or relationships to define the shear-layer velocity profile are confronted with unknown parameter limitations, such that their insights are difficult to adapt into a completely predictive tool. For example, Roshko provides a shear-layer velocity relationship to characterize bluff body wakes with the free-stream velocity  $U_\infty$  and the base-pressure coefficient  $C_{ps}$  [11]:

$$u = U_\infty \sqrt{1 - C_{ps}}. \quad (3)$$

Due to the fixed separation point of the shear-layer feeding an LEV, and their closed streamlines, there may be an analogy to the bluff body analysis of Roskko. However, even putting aside the effort to validate this analogy, it would be difficult to adapt as it would require the knowledge of the spanwise pressure profile. Indeed, knowing the pressure gradient distribution along a wing's surface would likely eliminate the need for a vortex growth model, as the ultimate goal of such models is often to predict lift.

Other studies have attempted to model the shear-layer velocity by the acceleration of the flow around the blockage effect of the LEV [12, 13]:

$$u = U_\infty \cdot \sin(\alpha_{\text{eff}}) \left( 1 + \frac{R_{\text{LEV}}^2(z, t)}{(R_{\text{LEV}} + d)^2} \right) + \frac{\Gamma(z, t)}{2\pi r_{\text{LEV}}} + \mathbf{u}_{\text{eff}}(z) \cdot \sin(\alpha_{\text{eff}}), \quad (4)$$

where  $d$  is the shear-layer thickness,  $R_{\text{LEV}}$  is the radius of the vortex area, and  $r_{\text{LEV}}$  represents the distance from the vortex center, as depicted in Fig. 1. This model has been independently applied to both rotating and flexible wings [12, 13]. The effective velocity  $\mathbf{u}_{\text{eff}}$  is the local flow velocity, which is evaluated with the rotational speed  $\Omega$  and the spanwise location from the axis of rotation  $z$  as  $\mathbf{u}_{\text{eff}} = \Omega \cdot z$  for the specific case of a wing in pure rotation, as will be investigated in this study.

This model requires modelling the vortex area itself, in addition to the circulation of the vortex. As circulation enters the LEV with mass through the leading-edge shear-layer, the relationship between area (or radius) and mass is straightforward via density:

$$R_{\text{LEV}}(t) = \sqrt{\frac{2}{\pi\rho} m'(t)}, \quad (5)$$

where the mass per unit span  $m'$  is evaluated by integrating the mass entering the vortex through the leading-edge shear layer, minus the mass removed through spanwise flow as:

$$m(t)|_z = \rho \int \left( d \frac{u_i + u_o}{2} \Delta z - \iint_A w(z, r, t) \cdot \mathbf{n} dA \right) dt, \quad (6)$$

where  $z$  is a spanwise position and  $\Delta z$  is a spanwise element analogous to a strip-theory calculation, which approximates an airfoil flow as a spanwise arrangement of locally two-dimensional flows [14]. The shear-layer velocity  $u$  is expressed by both the inner and outer shear-layer velocities  $u_i$  and  $u_o$ . This expression for the mass flux into the LEV includes an extra term to account for the mass transport due to spanwise flow. Here,  $w(z, r, t)$  represents the spanwise component of velocity and  $A$  represents the area of the LEV.

As the spanwise flow removes mass along the spanwise direction, it also removes circulation. The circulation transport can be determined by integrating the vorticity-transport equation over the vortex area. Taking an average across the vortex area, this value has been determined to be [5]:

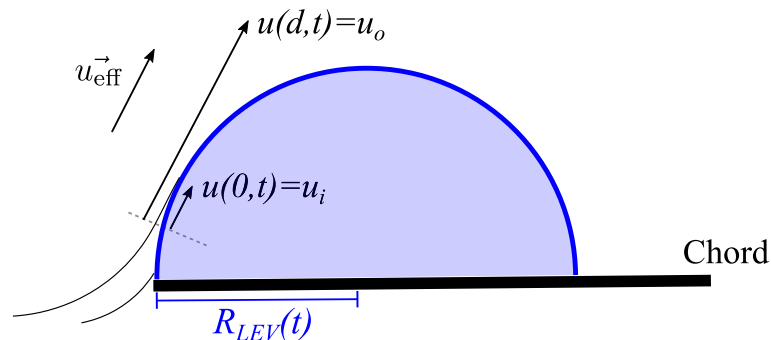


**Fig. 1** Integration approximated area for the velocity field around the boundary of the shear layer of a LEV, represented as a semi-cylinder of radius  $R_{\text{LEV}}(t, z)$

$$\frac{\partial \Gamma}{\partial t} = \overline{w} \frac{\partial \Gamma}{\partial z}, \tag{7}$$

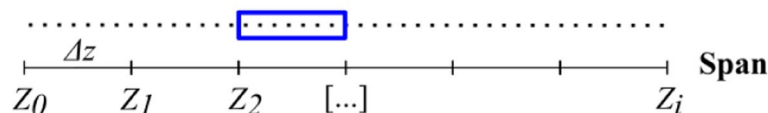
where the overbar here represents a spatial average. There are many ways to approach the implementation of the above equations as a predictive model. However, it is worth noting that by neglecting vortex tilting, we have already made the assumption that circulation follows the mass in the flow. This is a reasonable assumption far from the tip vorticities [15]. Therefore, we propose a particle-based model that tracks mass and circulation simultaneously. This combines previous work that either tracked only circulation [6], or tracked circulation and mass as distinct properties without such a particle-based approach, and includes implicitly the assumption above of low vortex tilting [12, 13]. In this way, we can de-couple the role of spanwise flow from the growth of circulation, and therefore model spanwise flow separately, as described in later sections.

### 1.2 Species transport model

Recent attempts to model the spanwise transport of circulation by species transport have proven helpful in accounting for the large number of unknowns in such a modelling process. However, these models attempted to track circulation alone. As the area of the LEV could not be computed with only circulation known, this limited the means by which the shear-layer velocity could be estimated. Here, we propose to adapt the shear-layer model presented in Section 1.1 to such particle-based models by tracking mass simultaneously.

The basic outline of the model is shown in Fig. 2. At each time step, particles representing mass are initialized uniformly across the wing span. Each particle is assigned a mass and circulation based on the shear-layer properties at that time step, and is then allowed to advect along the span, as shown in Fig. 3. As seen in Fig. 3, the fluid particles are advected along the span within a streamline in the LEV (identified as the blue helical streamline) and they are characterized by their mass and their circulation. For example, the fluid particle  $k$ , when crossing a plane of interest (identified by the green shaded area), is characterized by a mass  $M_k$  and a circulation  $\Gamma_k$ . At any given timestep, the total mass or circulation at a spanwise location is the sum of all the particles at that location — both those generated that time step, and those advected into that location over time.

Modelling the mass of the vortex with this particle-based method requires modifying the equations shown in Section 2. For instance, the mass flux into a spanwise section, shown in Eq. 6, no longer has to consider spanwise flow explicitly, as the motion of the particles will account for that. Therefore, particles are instead initialized by the value:

$$\begin{cases} M_k = \left(\frac{1}{2}u_o^2 \cdot d\right) \Delta t \Delta z \\ \Gamma_k = \frac{1}{2}u_o^2 \Delta t \end{cases}$$


**Fig. 2** At every time-step  $t$ ,  $N$  fluid particles representing vorticity-containing mass are initialized uniformly along the spanwise domain  $Z$  discretized in  $i$  bins. Each particle represented by the subscript  $k$  is initialized by the local mass  $M_k$  and circulation  $\Gamma_k$  divided equally among all the particles contained in the same bin

## Particles representing mass and circulation

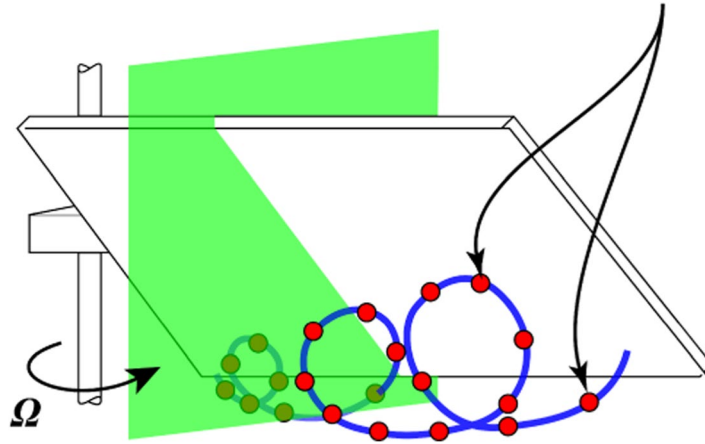


**Fig. 3** In the species transport model proposed here, an example streamline (shown as a continuous blue line), is replaced by discrete particles representing mass and circulation (shown as red dots). At any given spanwise location (represented here by a green plane), the total circulation is the sum of that contributed by each particle in that region

$$m(t)|_z = \rho \left( d \frac{u_i + u_o}{2} \Delta z \right) dt. \quad (8)$$

Meanwhile, the shear-layer velocity estimate in Eq. 4 was derived using a different method for determining circulation. Removing that term gives the shear-layer velocity as:

$$u(d, t)|_z = \mathbf{u}_{\text{eff}}(z) \cdot \sin(\alpha_{\text{eff}}) \left( 2 + \frac{R^2(z, t)}{r^2} \right). \quad (9)$$

As such, the only variable that the modeller must assign a value *a priori* is the shear-layer thickness  $d$  in order to assign an initial value to any given particle. We expect the model to be robust and insensitive to the parameter  $d$  variation. Indeed, an increase of the parameter  $d$  value leads to an increase of the mass flow rate, but also leads to a decrease in the vorticity of the shear-layer, such that the net impact of the parameter  $d$  on circulation is expected to equally cancel, which would satisfy Didden's relationship mentioned in Eq. 2. One therefore only requires a model for spanwise flow in order to model the entire LEV growth.

### 1.3 Spanwise flow circulation transport models

The circulation transport described in the previous section is sensitive to the spanwise flow. The spanwise flow component in the present work plays an important role as it defines mass-particle transport along the span. Previous studies have described the spanwise flow distribution in a LEV on a rotating wing considering both the centrifugal acceleration distribution and the pressure gradient along the span. Moreover, these terms appear to be coupled. For instance, Van Den Berg and Ellington suggested that the spanwise flow is governed by the dynamic pressure gradient resulting from the velocity

distribution along the span, itself generated by the centrifugal acceleration resultant from the rotation of the wing [16]. Following this idea, Maxworthy characterized the pressure gradient along the span for a quasi-steady LEV on a rotating wing [4]. Maxworthy's model determined the pressure gradient that resulted from both the centrifugal effects as well as the distribution of circulation. Unfortunately, Maxworthy's model may be better suited to retroactively investigate a flow than as a predictive model, since it requires the vortex area, which is one of the terms we seek to compute. While this model provides key insight into the flow within the LEV, it cannot be easily adapted to the present case.

Therefore, to estimate the magnitude of the spanwise flow distribution for a rotating wing, we will implement a simpler model.

## 2 Methodology

To validate the circulation growth model, we will test the predicted values against experimental results under matching flow conditions. Particle Image Velocimetry (PIV) is used to evaluate the flow field at several spanwise positions, as well as in the spanwise direction. In addition to validating the total circulation values, the PIV measurements can be used to evaluate the shear-layer velocity and spanwise flow estimates produced by the model.

### 2.1 Shear-layer velocity estimation

To model the circulation generation, the distribution of the shear-layer velocity must be estimated. As the characteristic shear-layer velocity profiles demonstrated the inner shear-layer velocity is small when compared to the outer shear-layer velocity, the outer shear-layer velocity is the primary value characterizing the shear-layer velocity itself at the leading-edge. Experimental velocity values are obtained by sampling the velocity at the location of maximum shear. Values were sampled at several locations along a line normal to the velocity vector at this location of maximum shear, and the maximum velocity along this line is taken as the outer shear-layer velocity.

### 2.2 Spanwise flow estimation

As mentioned previously, the present study wishes to model the spanwise flow distribution along the rotating wing as it plays an important role in the circulation advection. Previous studies have observed a helical streamline in the vortex core of an LEV [17]. In order to avoid modelling as many additional unknowns as possible, we will apply Bernoulli's equation to the present problem along the helical streamline, such as that shown in Fig. 3, to estimate spanwise flow. As we are applying Bernoulli's equation to a viscous flow, we do not expect perfect agreement. However, LEVs have been surprisingly well described by inviscid models in the past [18], and we will validate that approximation here as well. The spanwise flow distribution given by Bernoulli's equation in rotating coordinates for an inviscid flow is:

$$\frac{P}{\rho g} + \frac{w^2}{2g} - \frac{z^2 \Omega^2}{2g} = \text{const}, \quad (10)$$

where  $P$  represents the local pressure,  $g$  represents the gravitational acceleration and  $z$  represents the distance from the axis of rotation, such that  $Z_T$  would represent the wing tip position within that spanwise domain. Assuming the spanwise flow is zero at the axis of rotation, the constant on the right-hand side of Eq. 10 is just a reference pressure  $\frac{2}{\rho}P_0$ . Therefore, assuming a linear pressure gradient in the LEV [19], the equation becomes:

$$w^2 = \frac{2}{\rho} \frac{\partial P}{\partial z} z + \Omega^2 z^2, \quad (11)$$

where  $\Omega$  represents the physical rotational speed and where the difference in pressure between a point at  $z$  and the axis of rotation is  $\frac{\partial P}{\partial z} z$ . It will be shown later on that, at least for our case, the entire pressure gradient term is small, in which case the resulting spanwise flow can be reasonably modelled as:

$$w^2 = \Omega^2 z^2. \quad (12)$$

While this model is imperfect, of course, it is worth noting that previous results concerning LEV stability can be recovered despite its simplicity. For instance, if we take the spanwise transport of circulation, that is, the right-hand side of Eq. 7, and normalize  $\Gamma$  by  $U_\infty c = \Omega Z_T c$ , normalize the gradient in  $z$  by  $Z_T$ , and the spanwise flow by  $\Omega Z_T$ , then the normalization follows as:

$$\bar{w} \frac{\partial \Gamma}{\partial z} \rightarrow \left( \frac{\bar{w}}{\Omega Z_T} \right) \left( \frac{\partial \Gamma}{\partial z} \frac{Z_T}{(\Omega Z_T) c} \right) = \bar{w} \frac{\partial \Gamma}{\partial z} \frac{1}{(\Omega Z_T)^2} AR = \Pi_0, \quad (13)$$

where it is presumed that this spanwise transport of circulation forms a Pi group,  $\Pi_0 = f(\Pi_1, \dots)$ , characterized by the aspect ratio ( $AR = \frac{Z_T}{c}$ ) of the wing. Therefore, the dimensional transport of circulation should scale with  $1/AR$ , such that lower aspect ratios correspond to more stable LEVs, which corresponds to the findings of Lentink and Dickinson [20, 21].

### 2.3 Parameter space selection

The circulation growth model assumes limited vortex tilting, and therefore the parameter space has been selected in order to minimize the effect of tip vortices. A continuously rotating wing also generates a stable LEV, which, while not strictly required, does simplify the measurement process. Therefore, we will evaluate the model in the case of a thin flat plate in rotation, at an angle-of-attack of 45 degrees. The angle-of-attack, which is representative of instantaneous angles of attack achieved by small biological flyers, was selected such that a strong LEV would form consistently. Reynolds numbers are selected to be low ( $Re = 1000$  and  $Re = 2500$ ), in order to maximize the effect of viscosity in order to test the assumption that viscous effects were small. The Reynolds number is then defined as:

$$Re = \frac{\rho \Omega Z_T c}{\mu}, \quad (14)$$



such that the Reynolds numbers are evaluated at the wing tip, where  $\rho$  represents the density and  $\mu$  represents the water viscosity. The selected position is defined as the distance from the axis of rotation but will be referred to as their position from the root of the wing. Their values include the  $0.5c$  gap distance from the axis of rotation to the root of the wing. The wing has a chord of  $c = 50.8$  mm (2 in), a span of  $b = 210$  mm and a thickness of  $\tau = 3.2$  mm (1/8 in), giving an overall aspect ratio of 4. The wing was rotated within a cubic tank of  $1\text{ m}^3$ . The dimensions satisfy the wing clearance criteria described by Jones et al. [22].

The spanwise locations are all in the inner-half of the span, in order to minimize the effect of the tip vortex and, therefore, minimize the effect of vortex tilting. Measurements were therefore taken at  $1/4$ ,  $1/3$ , and  $1/2$  of the span length, from the root to the wing tip. The wing was rotated at a constant rate by a stepper motor. To achieve the low rotational speeds required by the selected Reynolds numbers, a 27:1 planetary gear reduction was placed between the stepper motor (Longrunner 22B, 200-step-per-revolution) and the drive shaft.

#### 2.4 Optical set-up

Two optical set-ups were used to capture the flow within the vortex core and the spanwise flow, respectively, as shown in Fig. 4. The PIV setup consists of a Photron FAST-CAM Mini WX-50 high-speed camera with a Tamron 100 mm/2.8 lens. A 6.5 W continuous wave-laser was used to illuminate the flow field, seeded with polymer microbeads of diameter  $50 \times 10^{-6}$  m. The image resolution was  $2048 \times 2048$  px<sup>2</sup> with a pixel size of  $10\mu\text{m}$  and a resolution of  $7.32 \times 10^{-2}$  mm/px. The field of view was approximately 150 mm for all test cases, with small variations between spanwise locations. The specific frame rate varied between individual test cases as a function of the local flow velocity. Vector fields were computed in LaVision Davis 10.

PIV measurements captured velocity fields to describe both the spanwise flow and to compute the circulation using separate laser planes. The spanwise flow data was captured when the span of the rotating wing was perpendicular to the camera's axis, where the laser sheet that illuminated the entire wing span was normal with the camera's axis and passed through the axis of rotation. Meanwhile, the velocity fields used to compute circulation were captured when the span of the rotating wing was parallel to the camera's axis. The laser sheet was again perpendicular with the camera's axis, such that in this case the laser plane was also normal to the wing span, and offset from the axis of rotation such that it would illuminate the desired spanwise location. The laser sheet's plane was moved for each spanwise location set of measurements.

Measurements were repeated at several azimuthal angles, in order to observe any time-dependence in the LEV strength or shear-layer velocity. The selected revolution angles range varies from 90 degrees to 225 degrees with increments of 45 degrees, such that effects from the impulsive start are excluded. Therefore, from here on, azimuthal angle and time may be used interchangeably. The wing started its rotation by being positioned with the desired revolution angle with the camera's axis, such that the camera trigger is synchronized with the azimuthal angle. As PIV images were collected continuously, individual azimuthal angles were selected from PIV images by comparing wing geometry to pre-determined known positions in the raw images.



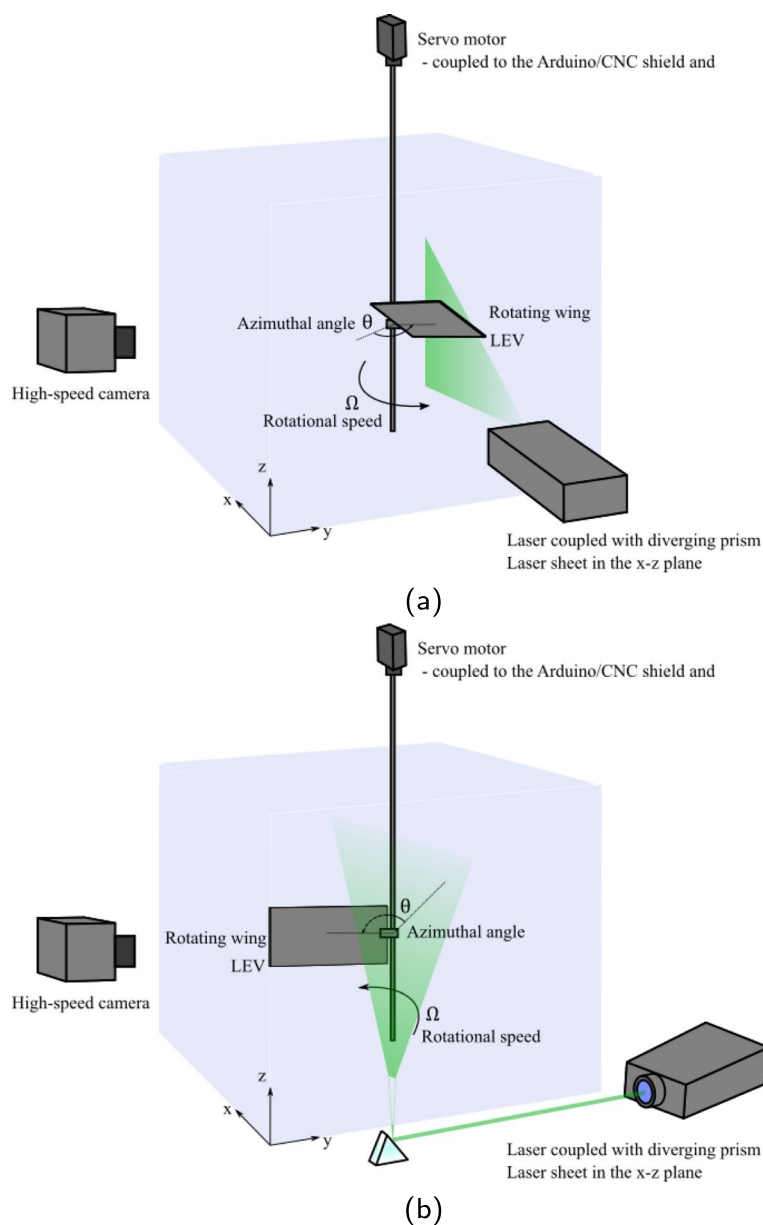


**Fig. 4** Experimental set-up for **a** the spanwise flow measurements and **b** the LEV circulation growth measurements. In both cases, the laser sheet plane is parallel to the camera, however in the first case **(a)**, the laser-sheet is centered with the axis of rotation; while in the second case **(b)**, the laser-sheet is centered with the spanwise location of interest. The high-speed camera also captures the velocity fields of the flow for different planes of interest. To measure the spanwise flow, the velocity fields are captured when the rotating wing is parallel with the camera's plane; and to compute the circulation, the velocity fields are captured when the rotating wing is perpendicular with the camera's plane

A median normalization was applied prior to vector calculation to subtract the background image for each run. Ten runs were recorded for each case. After the median normalization, only frames where the LEV presents perpendicular to the camera were kept to be processed. Flow fields were calculated with a multi-grid/multi-pass cross-correlation algorithm. For each study case, an overlap of 50% was applied to the first two passes

with the initial interrogation window and an overlap of 75% was applied to the last two passes. While symmetric interrogation windows such as squares and similar shapes are the most computationally efficient, asymmetric interrogation windows, such as ellipses, can provide greater dynamic range in areas of high shear and thus, best capture large velocity gradients in the shear-layer. Such asymmetric interrogation windows were utilized when optimization of PIV measurements was necessary, with their orientation and aspect ratio chosen automatically by the software based on velocities determined in the first pass of a multi-pass scheme.

A characteristic LEV structure is illustrated with the instantaneous vorticity field in Fig. 5a. Rather than selecting a threshold value to define the vortex, we intend to capture circulation near the wing, as defined geometrically in Fig. 5 by the control volume shown as a black rectangle containing the entire LEV region. In this figure, the vorticity distribution is extracted from direct measurements taken at the location 1/4 of the span for the  $Re = 1000$  test case and for the azimuthal angles of 90 degrees. However, for the purpose of showing the qualitative vortex shape and size, this case is representative of the others. Figure 5b presents the standard uncertainty of velocity from this case, and is,

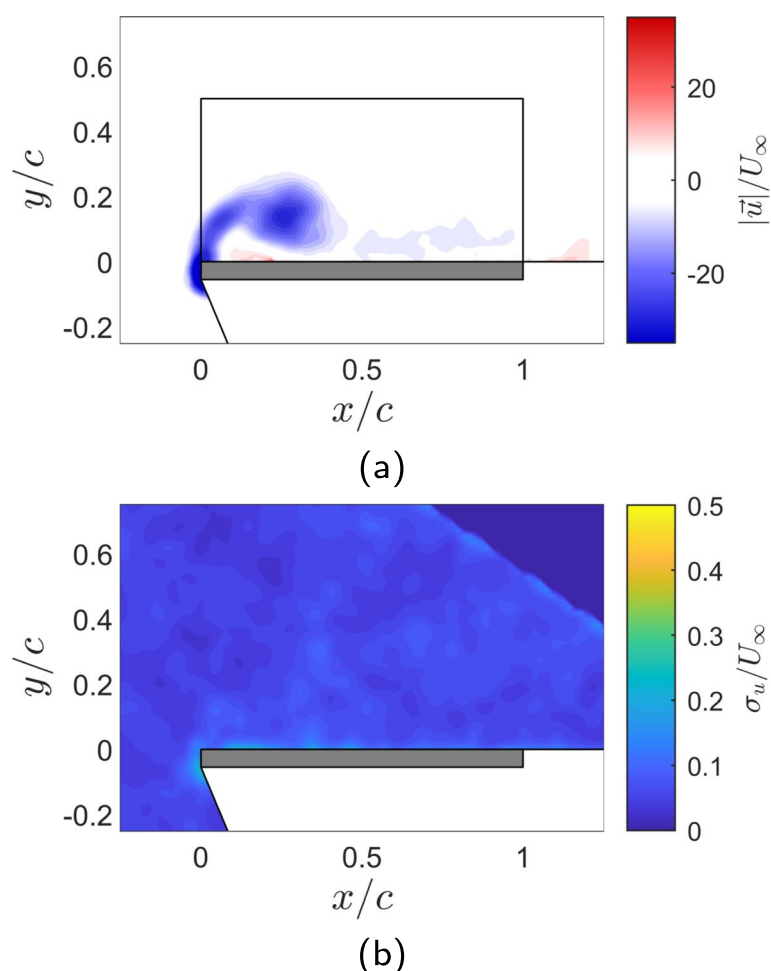
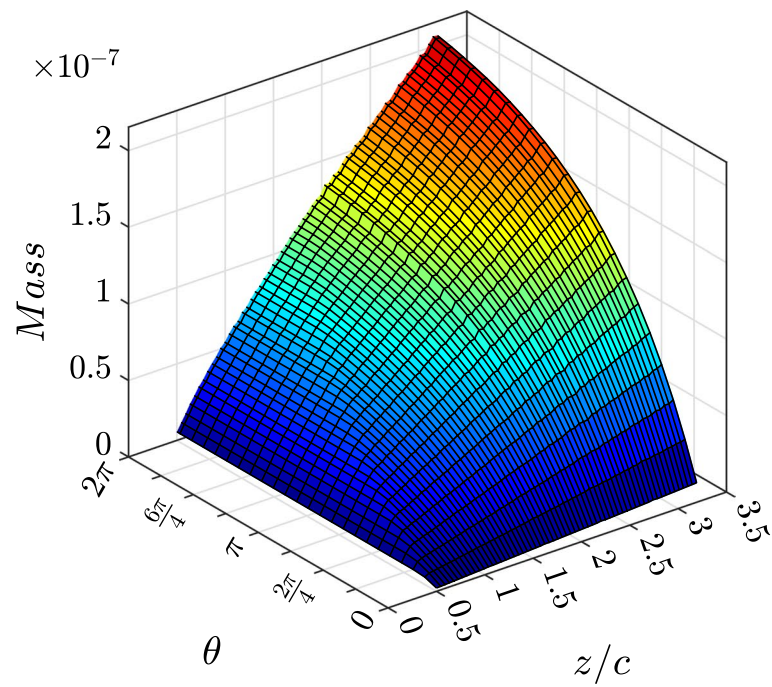
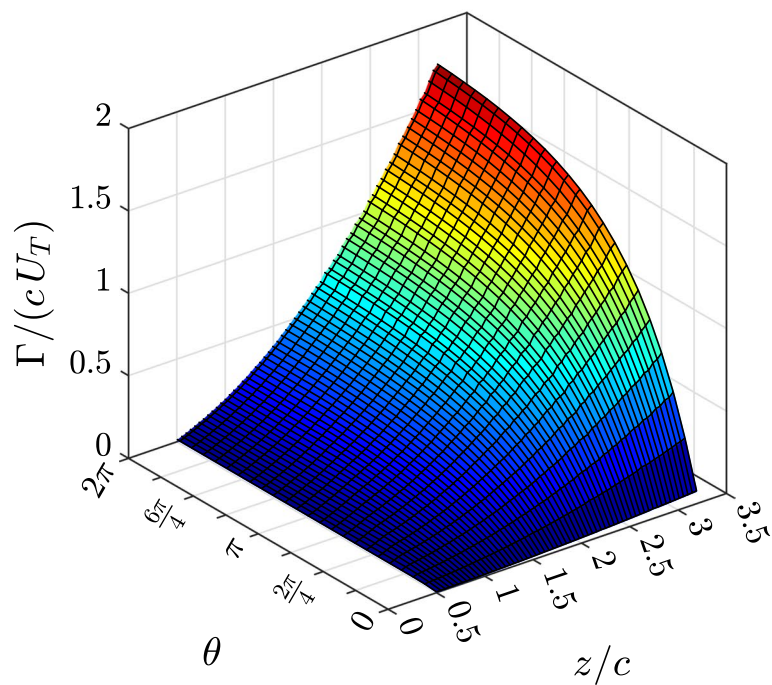


**Fig. 5** **a** A typical normalized vorticity field extracted from the quarter-span of the  $Re = 1000$  case, showing the integration window used to determine circulation. **b** The uncertainty of the PIV velocity vectors, normalized by the free-stream velocity



(a)



(b)

**Fig. 6** **a** The mass growth within the LEV along the span of a rotating wing is an approximately linear distribution while **b** the circulation growth along the span of a rotating wing is growing faster. Both the mass  $m$  and the circulation  $\Gamma^*$  distributions are presented in function of the span position  $z^*$  and in function of the time, or the equivalent revolution angle  $t^* = \theta$ . The figure presents the  $Re = 2500$  case, but the behaviours for the  $Re = 1000$  are similar

again, representative of others. PIV uncertainty was computed in LaVision Davis using the methods developed by Wieneke [23].

### 3 Results and discussion

Outputs from the model are presented in Fig. 6 for the  $Re = 2500$  case. The  $Re = 1000$  case is similar. As the model is tracking particles representing circulation-containing mass, the mass distribution within the LEV is presented as well in Fig. 6. As shown in Fig. 6, the distribution of mass into the LEV is approximately linear with the span while the circulation growth grows slightly faster along the span.

The circulation estimated by the model is compared to experimentally measured circulation values in Fig. 7. The experimental circulation values, computed directly from the velocity fields obtained from PIV measurements, are presented as broken lines. The predicted circulation values, generated by the model when inputting both spanwise flow and shear-layer velocity models, are presented as shaded ranges. The shaded region for the modelled values represents the range of circulation estimates obtained by varying the shear-layer thickness  $d$  by one order of magnitude, from  $d = 10^{-3}$  m to  $d = 10^{-2}$  m. As the shear-layer thickness is the only parameter the modeller can vary, this demonstrates that it has a negligible outcome on the output of the model. This is desirable, as the model is still useful without any *a priori* knowledge of the flow field, and the modeller only requires a rough guess of the shear-layer properties. Matching colors indicate identical spanwise position for easier visualisation. As shown in Fig. 7, the model is robust and minimally sensitive to the shear-layer thickness parameter input.

The modelled shear-layer velocity controls the circulation feeding term, while the modelled spanwise flow distribution controls the circulation transport. Eventually these terms find equilibrium, and the vortex is considered stable. However, the modelled circulation is in best agreement closer to the axis of rotation (1/4 and 1/3 of the span). This coincides to the regions along the span with the greatest agreement between modelled and measured spanwise flow, indicating that the quality of the spanwise flow model is the primary limiting factor in a circulation model of this type, which is discussed in the following section.

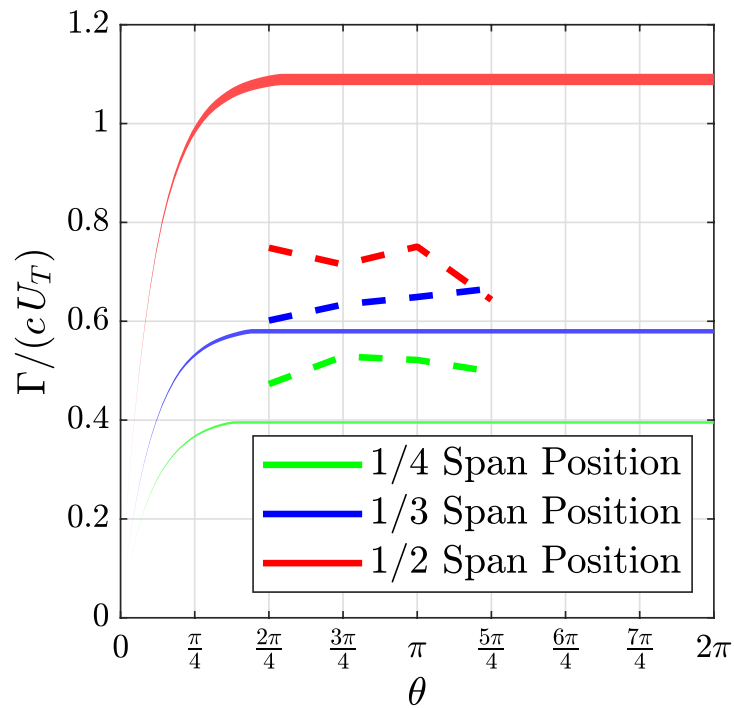
This similarity between the two test cases indicates that the viscous effects describing the LEV dynamics, such as those of the viscous diffusion, are small when compared to the convective effects, at least with respect to the strength of the LEV. This result is consistent with previous findings that the Reynolds number affects secondary structures around an LEV, but not the bulk circulation [24]. This suggests that the timescales characterizing the vortex growth are faster than those characterizing the viscous diffusion within the LEV.

#### 3.1 Spanwise flow approximation by Bernoulli's equation

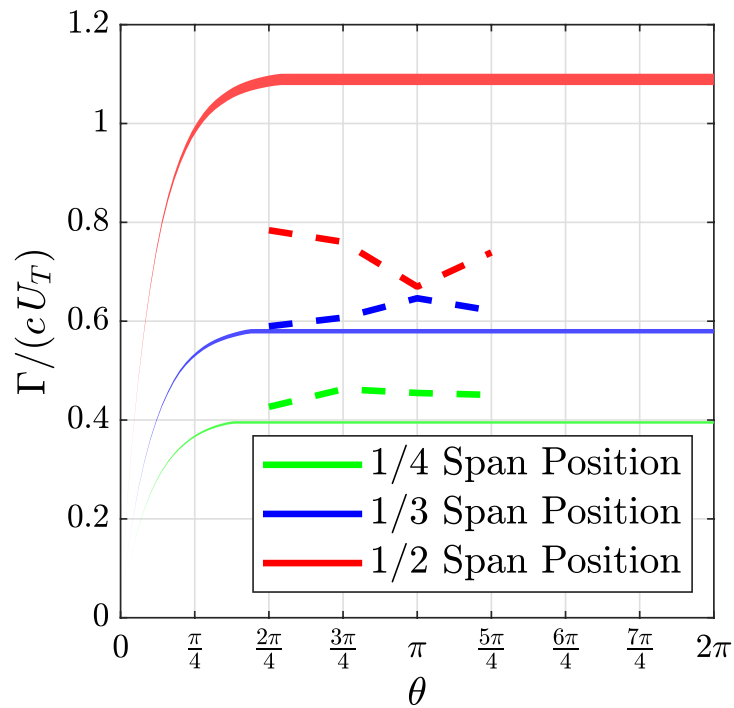
The experimental spanwise flow is shown in Fig. 8, alongside the modelled values. Fitting the modified Bernoulli equation to the experimental data, the pressure gradient term

(See figure on next page.)

**Fig. 7** Predicted circulation versus time for each spanwise position for **a**  $Re = 1000$  and **b**  $Re = 2500$ . The shaded area represents the prediction interval relative to the shear-layer thickness  $d$  parameter sensitivity. The predicted values are overall similar to the experimental circulation values and the circulation values predicted by the semi-empirical model. The behaviours for both Reynolds numbers are similar as the model was found to be insensitive to Reynolds numbers

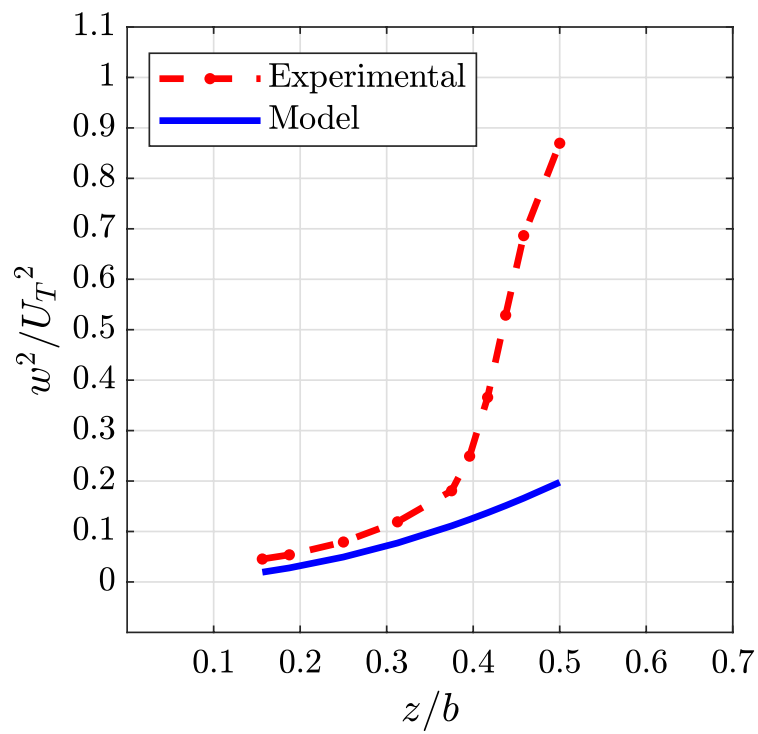


(a)

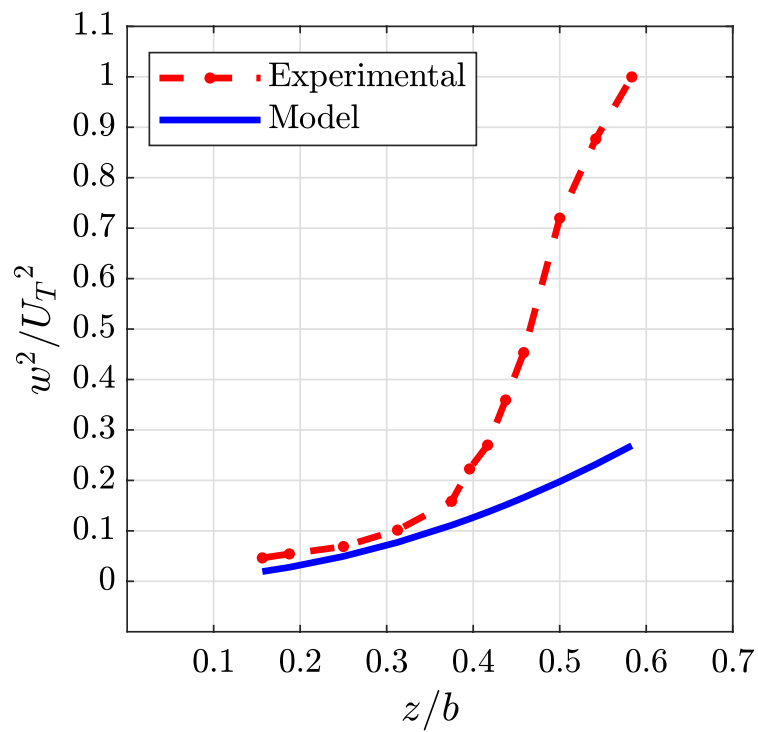


(b)

**Fig. 7** (See legend on previous page.)



(a)



(b)

**Fig. 8** Curve fits of the spanwise flow when constrained to match the form suggested from Bernoulli equation in rotating coordinates for **a**  $Re = 1000$ , and **b**  $Re = 2500$ . In both cases, the spanwise flow is primarily driven by rotational acceleration rather than the pressure gradient

contributes very little to the overall spanwise flow, using the rotational term contributing more than 95% of the total magnitude. While the Bernoulli equation in rotating coordinates estimates the magnitude of the spanwise flow with both rotational and pressure terms, fitting the equation terms to the experimental data shows that the spanwise flow is driven mostly by the rotational acceleration, and the pressure variation  $\partial P/\partial z$  represents less than 5% of the total spanwise flow.

The modelled values therefore include only the rotational components, based on the physical rotation rate of the wing. As seen in Fig. 8, the modelled spanwise flow values are initially a good fit with the experimental data, but deviate from the experimental data with increased span. This suggests that the pressure gradient role probably grows in importance further away from the axis of rotation, to the point where it is no longer negligible. This is the likely reason that the predicted circulation values in Fig. 6 are in good agreement closer to the axis of rotation, but are overestimated farther along the span. As the circulation transport depends directly on the spanwise flow, this results in the over-estimate of circulation by the model previously observed in Fig. 7. However, it also shows that the model performs adequately as long as the spanwise flow estimates are accurate.

### 3.2 Shear-layer velocity profile approximation

The modelled shear-layer velocity is compared to the experimental shear-layer velocity in Fig. 9 for both  $Re = 1000$  and  $Re = 2500$ . There is little difference between the Reynolds number cases, which was expected due to the insensitivity to Reynolds number on LEV topology seen in the literature [18, 24]. The experimental shear-layer velocity, shown as the blue dashed line, grows along the span. The modelled shear-layer velocity presented in the solid line is also a nearly-linear distribution along the span within the experimental range. While the modelled shear-layer velocity is somewhat under-estimated at the root of the wing, the values converge as we reach the half-span location. A primary goal in setting our shear-layer model was to minimize the number of free-parameters given to the modeller in order to highlight the limitations of the particle-based methodology, and we therefore believe that better agreement is possible in future models if this condition is relaxed. In general, the model is less sensitive to accurate shear-layer velocities and thicknesses than to spanwise flow values, and therefore we believe the values given here are acceptable for the purposes of the model.

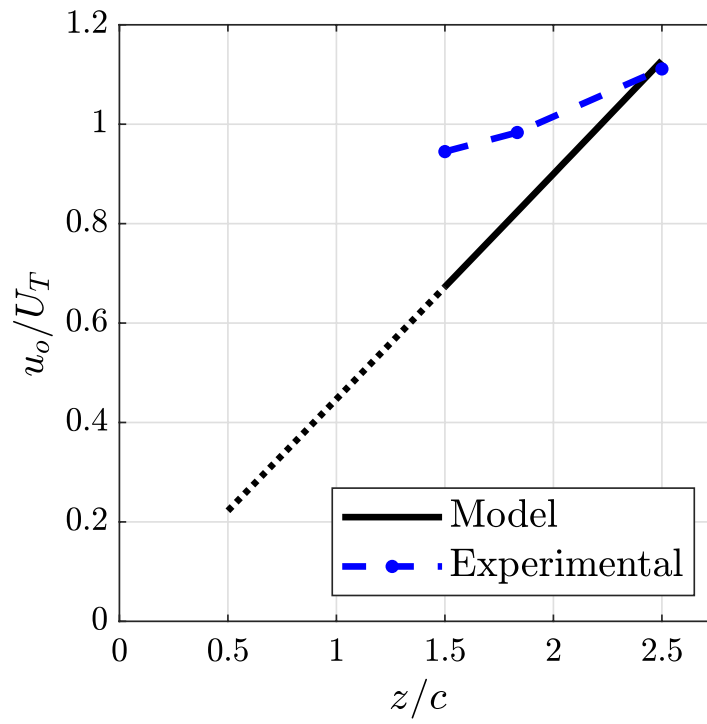
## 4 Conclusion

The purpose of this exercise was to provide a predictive model for the LEV circulation distribution along the span of a rotating wing. The model for spanwise circulation transport is derived from the approximation of the vorticity transport equation as species transport,

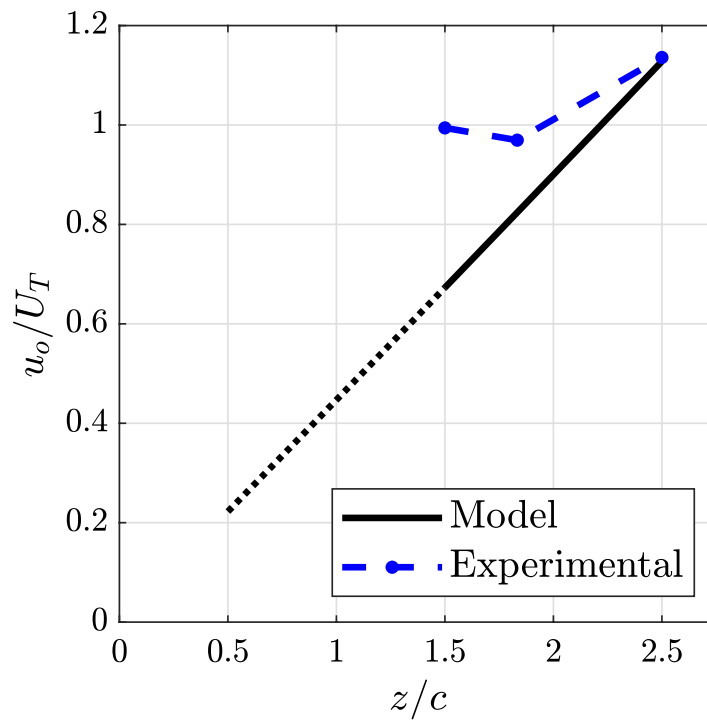
(See figure on next page.)

**Fig. 9** Predicted shear-layer velocity profile along the span versus experimental shear-layer velocity distribution (from 1/4 to 1/2 the span) for **a**  $Re = 1000$  and **b**  $Re = 2500$ . The predicted values are identified by a solid line only for the spanwise region of interest and become a dot line to represent the projected values of the spanwise region between the root and 1/4 of the span. When normalized by the wing tip velocity, the shear-layer velocity profiles for both Reynolds numbers are similar, if not identical





(a)



(b)

**Fig. 9** (See legend on previous page.)

such that circulation is tied to the mass entering the LEV's shear-layer. The model originally only accounted for circulation transport, and not mass transport, requiring the use of empirical values for the shear-layer velocity. The addition of mass transport to the model here permitted the use of a shear-layer model, reducing the dependence on empirical data.

When given an appropriate and accurate spanwise flow model, the transport model accurately predicted the circulation of an LEV. However, in regions where the spanwise flow model underestimated the spanwise velocity, circulation values were over-estimated as the spanwise transport of circulation was under-estimated. This shows the need for a better model for the spanwise flow in a leading-edge vortex. Nevertheless, the model proved to be a simple and effective methodology to estimate the LEV circulation growth along the span for a rotating wing, in situations where vortex tilting is not expected to be significant.

#### Acknowledgements

Not applicable.

#### Authors' contributions

Clara Morency developed and conducted the experiments presented in this article, under the supervision of Jaime Wong. The project was conceptualized by Jaime Wong. The text of this manuscript was produced equally by both authors. The authors read and approved the final manuscript.

#### Funding

This work was supported by the Natural Sciences and Engineering Research Council of Canada under grant No. RGPIN-2018-05168.

#### Availability of data and materials

The authors declare that data will be made available in a publicly-accessible repository upon acceptance of the manuscript.

#### Declarations

##### Competing interests

The authors declare that they have no competing interests.

Received: 25 July 2022 Accepted: 17 October 2022

Published online: 21 November 2022

#### References

- Rival D, Prangemeier T, Tropea C (2009) The influence of airfoil kinematics on the formation of leading-edge vortices in bio-inspired flight. *Exp Fluids* 46:823–833
- Rival D, Tropea C (2010) Characteristics of pitching and plunging airfoils under dynamic-stall conditions. *J Aircr* 47(1):80–86
- Rival DE, Kriegseis J, Schaub P et al (2014) Characteristic length scales for vortex detachment on plunging profiles with varying leading-edge geometry. *Exp Fluids* 55:1660
- Maxworthy T (2007) The formation and maintenance of a leading-edge vortex during the forward motion of an animal wing. *J Fluid Mech* 587:471–475
- Wong JG, Rival DE (2015) Determining the relative stability of leading-edge vortices on nominally two-dimensional flapping profiles. *J Fluid Mech* 766:611–625
- Wong JG, Gillespie G, Rival DE (2018) Circulation redistribution in leading-edge vortices with spanwise flow. *AIAA J* 56(10):3857–3862
- Didden N (1979) On the formation of vortex rings: rolling-up and production of circulation. *Z Angew Math Phys* 30:101–116
- Morton BR (1984) The generation and decay of vorticity. *Geophys Astrophys Fluid Dyn* 28(3–4):277–308
- Sattari P, Rival DE, Martinuzzi RJ et al (2012) Growth and separation of a start-up vortex from a two-dimensional shear layer. *Phys Fluids* 24(10):107102
- Wojcik CJ, Buchholz JHJ (2014) Vorticity transport in the leading-edge vortex on a rotating blade. *J Fluid Mech* 743:249–261
- Roshko A (1954) On the drag and shedding frequency of two-dimensional bluff bodies. NACA Tech Note NACA-TN-3169
- Wong JG, Kriegseis J, Rival DE (2013) An investigation into vortex growth and stabilization for two-dimensional plunging and flapping plates with varying sweep. *J Fluids Struct* 43:231–243
- Jia K, Scofield T, Wei M et al (2021) Vorticity transfer in a leading-edge vortex due to controlled spanwise bending. *Phys Rev Fluids* 6(2):024703
- Wright JR, Cooper JE (2008) Introduction to aircraft aeroelasticity and loads, vol 20. Wiley, New York

15. Cheng B, Sane SP, Barbera G et al (2013) Three-dimensional flow visualization and vorticity dynamics in revolving wings. *Exp Fluids* 54:1423
16. Van Den Berg C, Ellington CP (1997) The three-dimensional leading-edge vortex of a 'hovering' model hawkmoth. *Phil Trans R Soc Lond B* 352(1351):329–340
17. Linehan T, Mohseni K (2020) On the maintenance of an attached leading-edge vortex via model bird alula. *J Fluid Mech* 897:A17
18. Baik YS, Bernal LP, Granlund K et al (2012) Unsteady force generation and vortex dynamics of pitching and plunging aerofoils. *J Fluid Mech* 709:37–68
19. Limacher E, Morton C, Wood D (2016) On the trajectory of leading-edge vortices under the influence of Coriolis acceleration. *J Fluid Mech* 800:R1
20. Lentink D, Dickinson MH (2009) Biofluiddynamic scaling of flapping, spinning and translating fins and wings. *J Exp Biol* 212(16):2691–2704
21. Lentink D, Dickinson MH (2009) Rotational accelerations stabilize leading edge vortices on revolving fly wings. *J Exp Biol* 212(16):2705–2719
22. Manar F, Medina A, Jones AR (2014) Tip vortex structure and aerodynamic loading on rotating wings in confined spaces. *Exp Fluids* 55:1815
23. Wieneke B (2015) PIV uncertainty quantification from correlation statistics. *Meas Sci Technol* 26(7):074002
24. Garmann DJ, Visbal MR, Orkwis PD (2013) Three-dimensional flow structure and aerodynamic loading on a revolving wing. *Phys Fluids* 25:034101

### Publisher's Note

Springer Nature remains neutral with regard to jurisdictional claims in published maps and institutional affiliations.

**Submit your manuscript to a SpringerOpen<sup>®</sup> journal and benefit from:**

- ▶ Convenient online submission
- ▶ Rigorous peer review
- ▶ Open access: articles freely available online
- ▶ High visibility within the field
- ▶ Retaining the copyright to your article

---

Submit your next manuscript at ▶ [springeropen.com](https://www.springeropen.com)

---